American Mineralogist, Volume 80, pages 649–663, 1995

Thermodynamics and petrology of cummingtonite*

BERNARD W. EVANS, MARK S. GHIORSO
Department of Geological Sciences, Box 351310, University of Washington, Seattle, Washington 98195, U.S.A.

ABSTRACT

Natural cummingtonite encompasses virtually the entire compositional range from Mg to Fe end-member. It occurs in several metamorphic rock types, but predominantly in amphibolites and metaironstones. Most examples were produced under amphibolite-facies conditions, although the full range for cummingtonite is at least 400–800 °C and <1–15 kbar. Cummingtonite is also a critical indicator of T, a_{H_2O}, and f_{O_2} in silicic volcanic rocks from shallow magma chambers.

The solution properties of cummingtonite reflect the entropic and enthalpic consequences of temperature-dependent, long-range ordering of Mg and Fe^{2+} on the M1 + M3, M2, and M4 sites, plus modest site-mismatch energies. Solutions show small positive departure from ideal at 700–800 °C and both positive and negative behavior at lower temperatures depending on composition. The quenched state of M-site ordering has an influence on the symmetry of the unit cell ($C2/m$ vs. $P2_1/m$) and on the optical indicatrix. The kinetics of diffusion of Fe^{2+} and Mg among sites appears to be site dependent.

Magnesio-cummingtonite from 0 to about 10% grunerite is less stable than magnesian anthophyllite at metamorphic temperatures of 600–700 °C. The inversion loop in the system FMSH, with anthophyllite as the low-temperature form, probably has a minimum temperature close to the Fe end. The paragenesis of cummingtonite with olivine and quartz (found in metamorphosed iron formation) is confined to pressures below 10 kbar, temperatures below 740 °C, and f_{O_2} no more than 0.5 log unit above QFM. The paragenesis of cummingtonite with orthopyroxene and quartz typifies more Mg-rich compositions and generally signifies higher temperatures and in many instances higher pressures, and a temperature maximum (extremum) exists in the isobaric T-X_{Fe} diagram. The composition of cummingtonite together with magnetite, quartz, and H_2O fluid is a sensitive indicator of f_{O_2}. Cummingtonite must be Mg rich to coexist with hematite. Temperature and f_{O_2} determined from iron titanium oxide phenocrysts and measured cummingtonite compositions in rhyolites from the Taupo Zone, New Zealand, agree well with predicted relations. The agreement is less good for dacites from Saint Helens and Pinatubo. With increasing pressure, reactions between cummingtonite and the components of feldspar produce biotite and hornblende and restrict the occurrence of cummingtonite in amphibolites and systems of granitic composition.

INTRODUCTION

Rock-forming amphiboles have resisted attempts by petrologists to exploit them as petrogenetic indicators. Their compositions and parageneses are sensitive to many environmental parameters, and they occur very widely on Earth. The problem is a lack of quality data on the thermodynamic properties of amphibole end-members and their solutions, a situation that is compounded by their compositional complexity. What follows is a status report on our attempt to make a dent in the problem.

The ferromagnesian cummingtonite series is a logical starting point for a rigorous treatment of the thermodynamic properties of the amphiboles, especially for one that explicitly incorporates the energetic consequences of ordering of atoms on sites. The monoclinic ($C2/m$ and $P2_1/m$) magnesio-cummingtonite–cummingtonite–grunerite series is compositionally the simplest of the major groups of rock-forming amphibole. This has facilitated the collection by single-crystal methods of a set of data on the temperature and composition dependence of ordering of Mg and Fe^{2+} on the four M sites (Hirschmann et al., 1994). These data have been fitted by nonlinear least-squares methods and combined with standard-state properties and experimental brackets on a heterogeneous phase equilibrium to derive a set of thermodynamic solution properties of the ferromagnesian cummingtonite series (Ghiorso et al., 1995) that can be employed over its entire range of stability. Internal consistency with the thermodynamic data base of Berman (1988) has been

* Presented as part of the Presidential Address given by B. W. Evans at the annual meeting of the Mineralogical Society of America, October 25, 1994, in Seattle, Washington.

0003–004X/95/0708–0649$02.00

maintained. In this paper we explore some of the consequences of these data for parageneses of cummingtonite in a range of metamorphic and igneous environments. In a subsequent contribution we will derive a set of parameters for the thermodynamic properties of the entire amphibole quadrilateral that incorporates the cummingtonite data unchanged.

Composition and occurrence of cummingtonite

Natural members of the series appear to cover the entire range from the Mg end-member to the Fe end-member. In current terminology (Leake, 1978), magnesio-cummingtonite extends to the 30% Fe end-member composition, cummingtonite from 30 to 70%, and grunerite from 70 to 100%. Although intermediate and Fe-rich compositions predominate in nature, numerous examples of magnesio-cummingtonite in metamorphosed ultramafic rocks (with X_{Fe} ranging down to 0.08) have been reported in recent years (e.g., Kisch, 1969; Ross et al., 1969; Rice et al., 1974; Pfeifer, 1979; Matthes, 1986; Dymek et al., 1988; Droop, 1994). Furthermore, the "clinoanthophyllite" lamellae in tremolite described by Bown (1966) have been confirmed by Carpenter (1982) to be $P2_1/m$ magnesio-cummingtonite, exsolved from a virtually Fe-free host. Substitution of large amounts of Mn, leading to dannemorite, $Mn_2Fe_5Si_8O_{22}(OH)_2$, and tirodite, $Mn_2Mg_5Si_8O_{22}(OH)_2$, is found in cummingtonite from ferromanganese metasediments, but in most rock-forming cummingtonite the extent of exchange along the vectors $MnMg_{-1}$, $CaMg_{-1}$, $F,Cl(OH)_{-1}$, $Al_2(MgSi)_{-1}$ (**tk**), and $NaAl(\square Si)_{-1}$(**ed**), is limited. The cummingtonite and grunerite of metamorphosed iron formations tend to be particularly pure, with nonquadrilateral components less than 5% (Klein, 1982). In contrast to cummingtonite, orthorhombic (*Pnma*) anthophyllite is predominantly Mg rich and tends to be intermediate to Fe rich only when accompanied by coupled substitution along **tk** and **ed**, which eventually brings it (across a solvus below about 600 °C) into the range of gedrite. Mg-rich anthophyllite is typically low in Al and Ca.

Cummingtonite occurs widely in metamorphic rocks under conditions ranging from upper greenschist and blueschist-eclogite facies to beginning granulite facies. Whole-rock compositions must be within reach of the F corner in paragenesis diagrams such as the ACF triangle; thus, the most favorable lithological types for cummingtonite are iron formations, Ca-poor amphibolites, ultramafic rocks, and certain quartzofeldspathic rocks. Parageneses of cummingtonite include minerals such as clino- and orthopyroxene, olivine, pyralspite garnet, siderite, ankerite, calcite, calcic amphibole, orthoamphibole, cordierite, magnetite, hematite, minnesotaite, and deerite. These associations contribute greatly to the importance of cummingtonite as a petrogenetic indicator (e.g., Miyano and Klein, 1986). Cummingtonite-bearing amphibolites are commonest in relatively low-pressure environments, but in rocks lacking plagioclase and potassium feldspar, such as ironstones, the field of stability of cummingtonite extends to at least 15 kbar and overlaps that of deerite (Evans, 1986; Lattard and Le Breton, 1993). As a phenocryst phase in silicic volcanic rocks, cummingtonite provides information on f_{H_2O} and f_{O_2} as well as pressure and temperature. Cummingtonite is also found in plutonic rocks as a uralitic replacement of orthopyroxene and perhaps in some instances as a late magmatic phase (e.g., De Capitani and Liborio, 1990). Kenah and Hollister (1983) suggested that cummingtonite coexists with incipient melt in deep-crustal environments (in biotite-quartz-plagioclase gneiss), and Hoschek (1976) found cummingtonite to be a product of partial melting in material of similar composition. Thus, despite the bulk-compositional constraints, cummingtonite occurs in crustal rocks over a wide range of pressure and temperature conditions.

Homogeneous (intracrystalline) equilibrium

High-temperature Mg and Fe^{2+} site occupancies measured by single-crystal X-ray diffraction (Hirschmann et al., 1994) have been incorporated into a solution model that recognizes three energetically distinct M sites (M1 = M3, M2, and M4) and evaluates the contributions of intrasite interaction parameters, ordering energies, and reciprocal terms (Ghiorso et al., 1995). Calculated isotherms for ordering among pairs of sites (Fig. 1) show measurable differences as a function of temperature over the range 100–800 °C for ordering between the M1 and M4 sites and an increasing rate of ordering as a function of decreasing temperature for M1 vs. M2. Thus, the former pair provides a measure of ordering state at any equilibration temperature, whereas the latter (depending on macroscopic X_{Fe}) offers greater sensitivity at temperatures of equilibration below 300–400 °C.

Magnesio-cummingtonite has $P2_1/m$ symmetry at room temperature, but details of the temperature- and composition-dependent displacive inversion to $C2/m$ at elevated temperatures have yet to be clarified for ferromagnesian cummingtonite (cf. Prewitt et al., 1970). Some compositions of natural cummingtonite in the range 30–40% grunerite are C centered but are primitive when quenched after heat treatment to preserve a high-temperature ordering state (Yang and Hirschmann, 1995). Thus, the inversion appears to depend on the amount of Mg on the M4 site.

Superimposed on the Roozeboom plot for M-site ordering in cummingtonite (Fig. 1) are measured occupancies of seven samples of unheated natural cummingtonite from metamorphosed iron formations. These record apparent quench temperatures of mostly 300–400 °C for ordering across M1 and M4 and 100–300 °C for M1 vs. M2. The systematic differences between pairs for each sample seem to indicate real variations in the kinetics of interdiffusion of Mg and Fe across different site pairs. This topic deserves further study, however, since the differences are based on extrapolation from ordering measurements at 600–750 °C. The apparent quench temper-

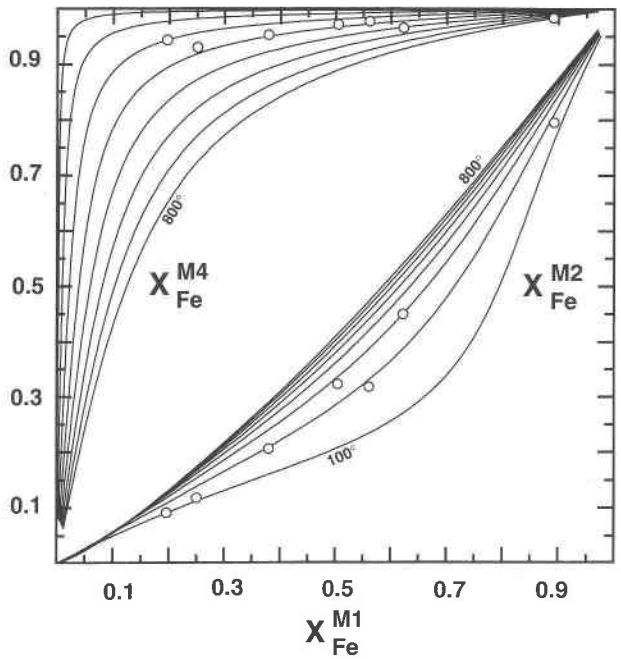

Fig. 1. Roozeboom plot of intracrystalline partitioning in binary ferromagnesian cummingtonite, with isotherms from Ghiorso et al. (1995, Fig. 1). $X_{Fe}^{M3} = X_{Fe}^{M1}$. Open circles are unheated, natural cummingtonite (from Hirschmann et al., 1994, and unpublished data).

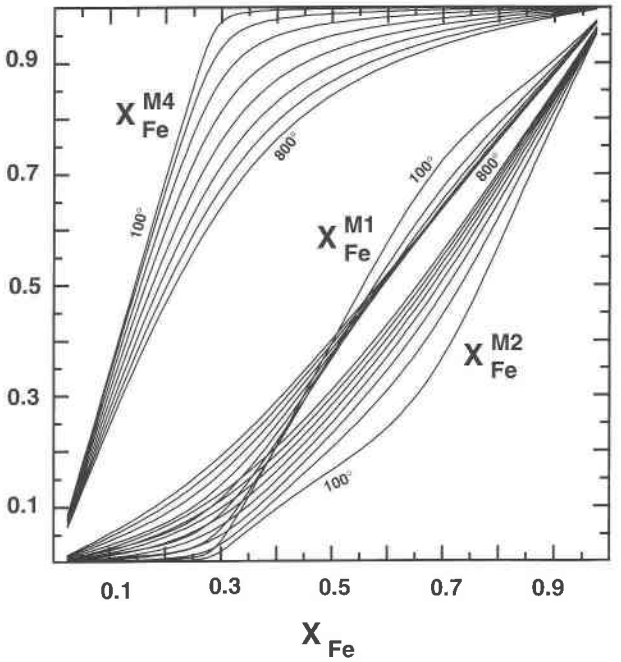

Fig. 2. Intracrystalline partitioning in binary ferromagnesian cummingtonite as a function of macroscopic X_{Fe}. Isotherms calculated after Ghiorso et al. (1995). Upper left and lower right parts of the diagram remain unoccupied at any temperature.

atures for M1 vs. M4 are broadly consistent with previous studies of the kinetics of M-site ordering in ferromagnesian amphiboles based on Mössbauer spectroscopy (Hafner and Ghose, 1971; Ghose and Weidner, 1972; Seifert and Virgo, 1975; Seifert, 1978).

Mössbauer spectroscopy is sensitive to compositional and temperature-dependent variations in Mg-Fe^{2+} ordering between the M4 and combined M123 sites in Al-poor ferromagnesian amphiboles, and it has supported cooling-rate studies (Seifert and Virgo, 1975). Some drawbacks of the technique for these minerals are (1) the sensitivity in ferroan cummingtonite and grunerite of X_{Mg} on M4 (calculated by difference from 1.0) to how measured Mn and Ca are assumed to be distributed among sites (Hirschmann et al., 1994, Fig. 8); (2) the probable need for a recoilless-free fraction correction (Grant and Dyar, 1994); (3) the requirement of several tens of milligrams of pure sample; and (4) the lack of information provided on the fractionation of Fe between M2 and M1 + M3. The X-ray single-crystal technique appears to offer additional insights into the kinetics of octahedral site ordering in ferromagnesian amphiboles. In principle, an independent chemical analysis of the single crystal is not needed (Hawthorne, 1983).

The refractive indices of orthopyroxene, as reflected in the optic axial angle, have been shown to be sensitive to the degree of Mg-Fe ordering (Tarasov and Nikitina, 1974; Tarasov et al., 1975; Besancon, 1991); indeed, $2V$ has long been known to differ for volcanic and plutonic orthopyroxene, and its value is symmetrical about X_{Fe} = 0.5. An analogous connection between order-disorder and optical properties also appears to be true for cummingtonite. Textbooks of optical mineralogy either rely on extrapolation or remain uncommitted regarding the optical properties of magnesio-cummingtonite, but we now know that the slopes of regression curves for the extinction angle $Z \wedge \mathbf{c}$ and optic axial angle $2V_z$ of natural cummingtonite change sign at the composition $X_{Fe} \approx 0.3$ (Medenbach and Evans, unpublished data), which is the approximate location of the bend over of the low-temperature isotherms in the Roozeboom plot (Figs. 1 and 2), where, with increasing macroscopic X_{Fe}, progressive filling of M4 by Fe changes to progressive filling of M1, M2, and M3 by Fe. Thus, whereas cummingtonite is optically positive, magnesio-cummingtonite is in part optically negative. The same behavior for synthetic fluor-cummingtonite was observed for $Z \wedge \mathbf{c}$ by Bowen and Schairer (1935). Work is in progress to see if volcanic cummingtonite and cummingtonite reequilibrated at high temperature differ in optical properties from low-temperature, ordered cummingtonite.

Solution properties of cummingtonite

The combination of strong M-site preferences and uneven (2, 2, 1, 2) amphibole site multiplicities is responsible for pronounced asymmetry in the solution properties of cummingtonite, especially at low temperatures. Our model (Ghiorso et al., 1995) incorporates measured values of configurational entropy at 600–750 °C and assumes complete disorder at infinite temperature and total

ordering of Fe on M4 and of Mg on M2 at 0 K. The temperature dependence of G, H, and S of mixing derives entirely from the temperature dependence of the configurational entropy; all eight fit parameters in the expression for the vibrational component of Gibbs energy of mixing are constants independent of temperature and pressure. The result is a partial cancellation of the entropic and enthalpic consequences of ordering, particularly at 700–800 °C where solutions behave in a slightly positive manner. Towards lower temperatures, solution behavior becomes more complex, with both positive and negative departures from ideal depending on macroscopic composition (Ghiorso et al., 1995, Fig. 11).

Computation of end-member activities

Computing activities of cummingtonite end-members is a two-step process. First, an equilibrium state of cation ordering must be calculated for a specified bulk composition and temperature. Second, this cation distribution must be used to compute the activity, a (or more precisely $RT \ln a$), of a given end-member component.

The first step is the most demanding. The given bulk composition of cummingtonite is first projected onto the Fe-Mg binary join and expressed as the mole fraction of the Fe end-member, X_{Fe}. Then, for a specified temperature, the following three equations are solved simultaneously for the site mole fractions X_{Fe}^{M13}, X_{Fe}^{M2}, and X_{Fe}^{M4}:

$$X_{Fe} = \frac{3X_{Fe}^{M13} + 2X_{Fe}^{M2} + 2X_{Fe}^{M4}}{7}$$

$$\begin{aligned}0 = {} & \Delta\overline{G}^{0}_{ORD,13} + \frac{6}{7}RT \ln\left[\left(\frac{X_{Mg}^{M13}}{X_{Fe}^{M13}}\right)^{2}\left(\frac{X_{Fe}^{M2}}{X_{Mg}^{M2}}\right)\left(\frac{X_{Fe}^{M4}}{X_{Mg}^{M4}}\right)\right] \\ & + \frac{4}{7}\left(3W_{13} + \frac{1}{2}\Delta\overline{G}^{0}_{X,13,24}\right)(X_{Fe}^{M13} - X_{Mg}^{M13}) \\ & - \frac{3}{7}\left(2W_{2} + \frac{1}{2}\Delta\overline{G}^{0}_{X,134,2}\right)(X_{Fe}^{M2} - X_{Mg}^{M2}) \\ & - \frac{3}{7}\left(2W_{4} + \frac{1}{2}\Delta\overline{G}^{0}_{X,123,4}\right)(X_{Fe}^{M4} - X_{Mg}^{M4}) \\ & + \frac{1}{2}(X_{Fe}^{M4} - X_{Fe}^{M13})\Delta\overline{G}^{0}_{X,13,24} \\ & + \frac{1}{2}(X_{Fe}^{M4} - X_{Fe}^{M2})(\Delta\overline{G}^{0}_{X,123,4} - \Delta\overline{G}^{0}_{X,134,2})\end{aligned}$$

$$\begin{aligned}0 = {} & \Delta\overline{G}^{0}_{ORD,2} + \frac{2}{7}RT \ln\left[\left(\frac{X_{Fe}^{M13}}{X_{Mg}^{M13}}\right)^{3}\left(\frac{X_{Mg}^{M2}}{X_{Fe}^{M2}}\right)^{5}\left(\frac{X_{Fe}^{M4}}{X_{Mg}^{M4}}\right)^{2}\right] \\ & - \frac{2}{7}\left(3W_{13} + \frac{1}{2}\Delta\overline{G}^{0}_{X,13,24}\right)(X_{Fe}^{M13} - X_{Mg}^{M13}) \\ & + \frac{5}{7}\left(2W_{2} + \frac{1}{2}\Delta\overline{G}^{0}_{X,134,2}\right)(X_{Fe}^{M2} - X_{Mg}^{M2}) \\ & - \frac{2}{7}\left(2W_{4} + \frac{1}{2}\Delta\overline{G}^{0}_{X,123,4}\right)(X_{Fe}^{M4} - X_{Mg}^{M4}) \\ & + \frac{1}{2}(X_{Fe}^{M4} - X_{Fe}^{M2} + X_{Fe}^{M13} - X_{Fe}^{M2})\Delta\overline{G}^{0}_{X,134,2} \\ & - \frac{1}{2}(X_{Fe}^{M4} - X_{Fe}^{M13})(\Delta\overline{G}^{0}_{X,13,24} - \Delta\overline{G}^{0}_{X,123,4})\end{aligned}$$

where X_{Mg}^{M13}, X_{Mg}^{M2}, and X_{Mg}^{M4} are given by $1 - X_{Fe}^{M13}$, $1 - X_{Fe}^{M2}$, and $1 - X_{Fe}^{M4}$, respectively. The last two of these expressions are taken from Table 5 of Ghiorso et al. (1995) and describe the state of homogeneous or internal equilibrium in the mineral. Numerical values of the thermodynamic model parameters found in the above expressions, $\Delta\overline{G}^{0}_{ORD,13}$, $\Delta\overline{G}^{0}_{ORD,2}$, $\Delta\overline{G}^{0}_{X,13,24}$, $\Delta\overline{G}^{0}_{X,134,2}$, $\Delta\overline{G}^{0}_{X,123,4}$, W_{13}, W_2, and W_4, are given in Table 9 of Ghiorso et al. (1995). The second and third expressions are nonlinear in the site mole fractions and pose something of a challenge for evaluation by pocket calculator. We provide a graphical solution of these three equations in Figure 2. This graphical evaluation should suffice for most applications. For those wishing to find solutions analytically, Newton-Raphson's method with derivatives (Press et al., 1990, p. 270–275) is the algorithm preferred by the authors.

Once site mole fractions corresponding to the equilibrium cation distribution are computed, then $RT \ln a$ for each end-member may be evaluated from expressions given by Ghiorso et al. (1995) and reproduced below. The activity of the Mg end-member, magnesio-cummingtonite, is given by

$$\begin{aligned}RT \ln a_{Cum} = {} & RT(3 \ln X_{Mg}^{M13} + 2 \ln X_{Mg}^{M2} + 2 \ln X_{Mg}^{M4}) \\ & + \left(3W_{13} + \frac{1}{2}\Delta\overline{G}^{0}_{X,13,24}\right)X_{Fe}^{M13}X_{Fe}^{M13} \\ & + \left(2W_{2} + \frac{1}{2}\Delta\overline{G}^{0}_{X,134,2}\right)X_{Fe}^{M2}X_{Fe}^{M2} \\ & + \left(2W_{4} + \frac{1}{2}\Delta\overline{G}^{0}_{X,123,4}\right)X_{Fe}^{M4}X_{Fe}^{M4} \\ & - \frac{1}{2}(X_{Fe}^{M4} - X_{Fe}^{M13})(X_{Fe}^{M2} - X_{Fe}^{M13})\Delta\overline{G}^{0}_{X,13,24} \\ & - \frac{1}{2}(X_{Fe}^{M2} - X_{Fe}^{M13})(X_{Fe}^{M2} - X_{Fe}^{M4})\Delta\overline{G}^{0}_{X,134,2} \\ & - \frac{1}{2}(X_{Fe}^{M4} - X_{Fe}^{M2})(X_{Fe}^{M4} - X_{Fe}^{M13})\Delta\overline{G}^{0}_{X,123,4}\end{aligned}$$

and that of the Fe end-member, grunerite, by

$$\begin{aligned}RT \ln a_{Gru} = {} & RT(3 \ln X_{Fe}^{M13} + 2 \ln X_{Fe}^{M2} + 2 \ln X_{Fe}^{M4}) \\ & + \left(3W_{13} + \frac{1}{2}\Delta\overline{G}^{0}_{X,13,24}\right)X_{Mg}^{M13}X_{Mg}^{M13} \\ & + \left(2W_{2} + \frac{1}{2}\Delta\overline{G}^{0}_{X,134,2}\right)X_{Mg}^{M2}X_{Mg}^{M2} \\ & + \left(2W_{4} + \frac{1}{2}\Delta\overline{G}^{0}_{X,123,4}\right)X_{Mg}^{M4}X_{Mg}^{M4} \\ & - \frac{1}{2}(X_{Fe}^{M4} - X_{Fe}^{M13})(X_{Fe}^{M2} - X_{Fe}^{M13})\Delta\overline{G}^{0}_{X,13,24}\end{aligned}$$

$$-\frac{1}{2}(X_{Fe}^{M2} - X_{Fe}^{M13})(X_{Fe}^{M2} - X_{Fe}^{M4})\Delta\overline{G}^{0}_{X,134,2}$$

$$-\frac{1}{2}(X_{Fe}^{M4} - X_{Fe}^{M2})(X_{Fe}^{M4} - X_{Fe}^{M13})\Delta\overline{G}^{0}_{X,123,4}.$$

A plot of activity-composition relations in cummingtonite is provided in Figure 11 of Ghiorso et al. (1995).

Cummingtonite vs. anthophyllite

Compositional overlap of natural cummingtonite and Al-poor anthophyllite apparently extends up to about $X_{Fe} = 0.5$ (e.g., Schneidermann and Tracy, 1991). Generally, intermediate to Fe-rich anthophyllite is aluminous. Mg end-member anthophyllite has for a long time been assumed to be more stable than the monoclinic analogue, and this conclusion is supported by a compilation of polybaric and polythermal Fe-Mg–exchange equilibrium data from natural pairs (Fig. 3). As both X_{Fe} and wt% Al_2O_3 approach zero, ln K_D for the exchange reaction tends to −0.125. Assuming Raoult's Law behavior of phase components for Mg-rich compositions in the equilibrium

$$\underset{\text{anthophyllite}}{Mg_7Si_8O_{22}(OH)_2} = \underset{\text{cummingtonite}}{Mg_7Si_8O_{22}(OH)_2} \qquad (1)$$

one can derive from this a rounded ΔG^0 at 650 °C for Equilibrium 1 of 1.0 kJ/mol. We use this difference to establish the thermodynamic properties of end-member magnesio-cummingtonite from those of magnesian anthophyllite (Ghiorso et al., 1995).

Unlike anthophyllite, magnesio-cummingtonite in metamorphic ultramafic rocks coexists in nearly all cases with tremolite, and contains more CaO than anthophyllite (Evans, 1982). Currently, we lack the data to derive the solution properties of Al-free ferromagnesian anthophyllite, but provisional calculations suggest that at about 650 °C the preferential uptake of Fe and Ca by cummingtonite results in stabilization of cummingtonite at $X_{Fe} > 0.06$–0.10. Anthophyllite, the lower temperature form, is stable to more Fe-rich compositions at lower temperatures. The isopleths for X_{Fe} in Figure 3, if correct, show that Mg-Fe partitioning between Al-free anthophyllite and cummingtonite reverses as X_{Fe} approaches 1.0. Therefore, the transition loop in the T-X_{Fe} section has a minimum T towards the Fe end, thereby resembling that for orthopyroxene *Pbca* vs. clinopyroxene *C2/c* (Sack and Ghiorso, 1994, Fig. 7). This behavior also means that the solution properties of binary ferromagnesian cummingtonite and anthophyllite are not identical. A comparison of Mg-Fe partitioning between olivine + cummingtonite and olivine + anthophyllite pairs from the literature (not shown here) confirms the dependence of ln K_D on X_{Fe} that is shown in Figure 3.

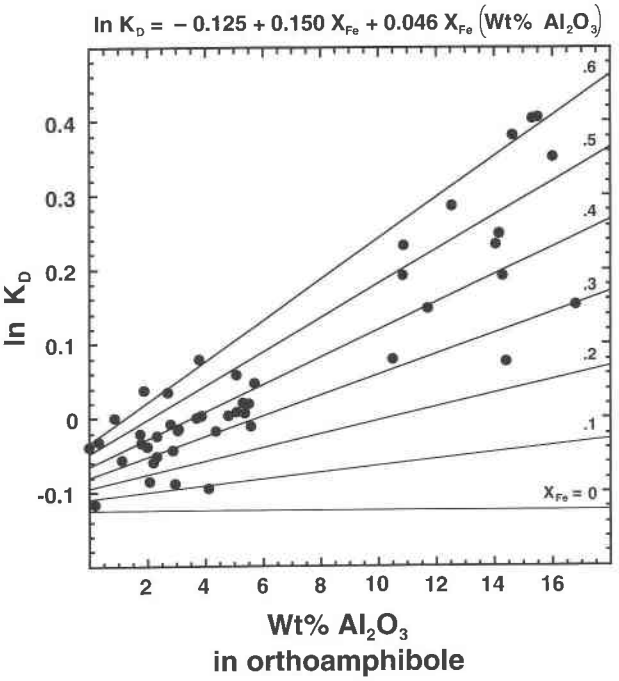

Fig. 3. Compilation from the literature of polythermal and polybaric Fe-Mg exchange equilibrium in natural monoclinic + orthorhombic Fe-Mg amphibole pairs, expressed as ln K_D vs. wt% Al_2O_3 in orthoamphibole and contoured for X_{Fe} in the orthoamphibole. Least-squares fit assumes no dependence of ln K_D on Al_2O_3 for Fe-free compositions.

Heterogeneous equilibrium with olivine, orthopyroxene, quartz, and H_2O fluid

In Ghiorso et al. (1995), end-member and solution properties of ferromagnesian cummingtonite were derived with reference to the end-member data for olivine, orthopyroxene, quartz, and magnetite tabulated by Berman (1988) and the solution model of Sack and Ghiorso (1989) for orthopyroxene. Calculated phase relations were shown to agree well with exchange, dehydration, and redox equilibrium experiments, particularly those of V. I. Fonarev and coworkers (Fonarev, 1987), and with coexisting natural mineral pairs in the literature. We explore here some further consequences of our new data on cummingtonite as they apply to certain metamorphic and magmatic systems.

The equilibrium of cummingtonite with olivine, quartz, and H_2O is confined to pressures lower than 10 kbar and temperatures lower than 740 °C (Fig. 4). The strong fractionation of Fe^{2+} and Mg between Fe-rich cummingtonite and fayalitic olivine results in a steep isobaric T-X_{Fe} phase loop (Fig. 5). Field descriptions of metamorphosed, banded iron formation are consistent with these phase diagrams in that olivine, always very Fe rich, is typically found as a breakdown product of grunerite in contact metamorphic environments and low-pressure regional metamorphic environments (compare Fig. 5A with 5B and 5C), as described, for example, in Bonnichsen (1969), Morey et al. (1972), Simmons et al. (1974), Floran and Papike (1978), Vaniman et al. (1980), and Haase (1982a, 1982b), Gole and Klein (1981), and Savko (1994), respectively. Given bulk compositions with extremely high Fe/Mg ratios, fayalite + quartz can of course occur at higher pressures (e.g., 5–6 kbar in iron formation: Berg,

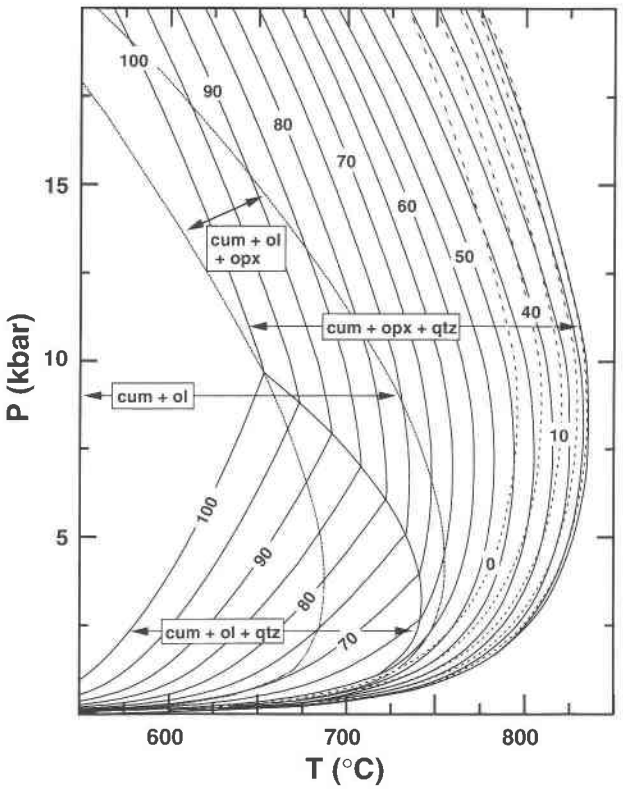

Fig. 4. *P-T* phase diagram showing the calculated stability limit of cummingtonite (as isopleths of X_{Fe} in cummingtonite) with respect to quartz, H_2O, and orthopyroxene (at high *P* and *T*) and olivine (at low *P* and *T*). Dashed lines are isopleths in the magnesio-cummingtonite range. Note that at high *P* magnesio-cummingtonite is metastable with respect to talc + orthopyroxene.

1977; Sharp and Essene, 1991; and 7–8 kbar in metagranites: Bohlen and Essene, 1978) up to the stability limit for the end-member (Bohlen et al., 1980).

The equilibrium of cummingtonite with orthopyroxene, quartz, and H_2O fluid occurs at higher temperatures than the analogous olivine equilibrium and is favored by pressure and higher Mg/Fe bulk compositions (Figs. 4 and 5). In addition, equilibrium temperatures are less strongly dependent on X_{Fe}. Indeed, cummingtonite and orthopyroxene have an azietropic relationship ($\ln K_D = 0$), which manifests itself as an isobaric temperature maximum (extremum) in the breakdown of cummingtonite to orthopyroxene, quartz, and H_2O (Fig. 5). The composition of the extremum is by coincidence quite close to the ordered amphibole composition, $Fe_2Mg_5Si_8O_{22}(OH)_2$ ($X_{Fe} = 0.29$), which becomes greatly stabilized at low temperatures (Ghiorso et al., 1995, Fig. 10); the calculated extremum composition varies from about $X_{Fe} = 0.30$ at 1 kbar to $X_{Fe} = 0.20$ at 20 kbar. The existence of this extremum is predicted by the thermodynamic modeling and confirmed independently by the compositions of coexisting cummingtonite, orthopyroxene, and olivine from metamorphosed ultramafic rocks (Fig. 6). From exchange experiments, Fonarev (1987, Figs. 64 and 67) also predicted this extremum but at temperatures less than about 750 °C, where, for all but the lowest metamorphic pressures, equilibrium would require a reduced activity of H_2O. This equilibrium serves as a model for prograde and retrograde reactions in a broad range of lithological types in high-amphibolite and granulite facies metamorphic environments (ironstones, Ca-poor amphibolites, metagreywackes, acid to intermediate orthogneisses) and for assemblages in silicic volcanics and probably some plutonic rocks.

For example, in amphibolites in central Massachusetts, reactions terminal to cummingtonite, including the orthopyroxene-forming reaction Cum = Opx + Hbl + Qtz + H_2O, have been carefully studied in the context of independent thermobarometry and regional isograds. A recent discussion of this is given by Hollocher (1991), who summarized relationships in a T-X_{Fe} diagram for an estimated 6 kbar lithostatic pressure. If we take his temperature estimates literally (an uncertainty of ±50 °C is suggested), our data would indicate that the metamorphism of amphibolite took place under conditions of H_2O activity of about 0.25–0.28 (Fig. 7).

In the system FeO-MgO-SiO_2-H_2O, cummingtonite, olivine, orthopyroxene, and H_2O may coexist in divariant equilibrium in the absence of quartz (Fig. 4), although over a very narrow temperature range for any given bulk composition (Fig. 5). (For very Mg-rich compositions this assemblage is metastable with respect to the analogous anthophyllite equilibrium.) This cummingtonite breakdown assemblage, which is found in metamorphosed ultramafic rocks, occurs at lower temperatures than the quartz-present breakdown of cummingtonite to orthopyroxene (Fig 5); this behavior is similar to that of tremolite and the reverse of what is more commonly the case for dehydration reactions in metamorphic petrology. Except for the more Mg-rich bulk compositions, the temperature of the quartz-absent equilibrium is virtually independent of X_{Fe}. The peculiarities of Fe-Mg partitioning among cummingtonite, olivine, and orthopyroxene (Fig. 6) result at high pressures (and low temperatures) in double maxima in the individual T-X_{Fe} curves for the minerals (Fig. 5D).

The FMSH univariant assemblage cummingtonite + olivine + orthopyroxene + quartz + H_2O possesses a temperature maximum in the *P-T* plane, and we compute this to be at about 3 kbar (Fig. 4). Fonarev (1987, Fig. 62) found a maximum at 4 kbar or nearer 3 kbar for $a_{H_2O} < 1.0$.

Lattard and Evans (1992, Fig. 9) showed that most high-grade regionally metamorphosed ironstones, in spite of their having earlier contained carbonate minerals, can be considered to have equilibrated under conditions of relatively high H_2O activity. This conclusion is unchanged when the new solution data are used. It is perhaps indicative of significant flux of H_2O-rich fluid through these rocks at some stage in their metamorphic evolution (e.g., Ferry, 1994).

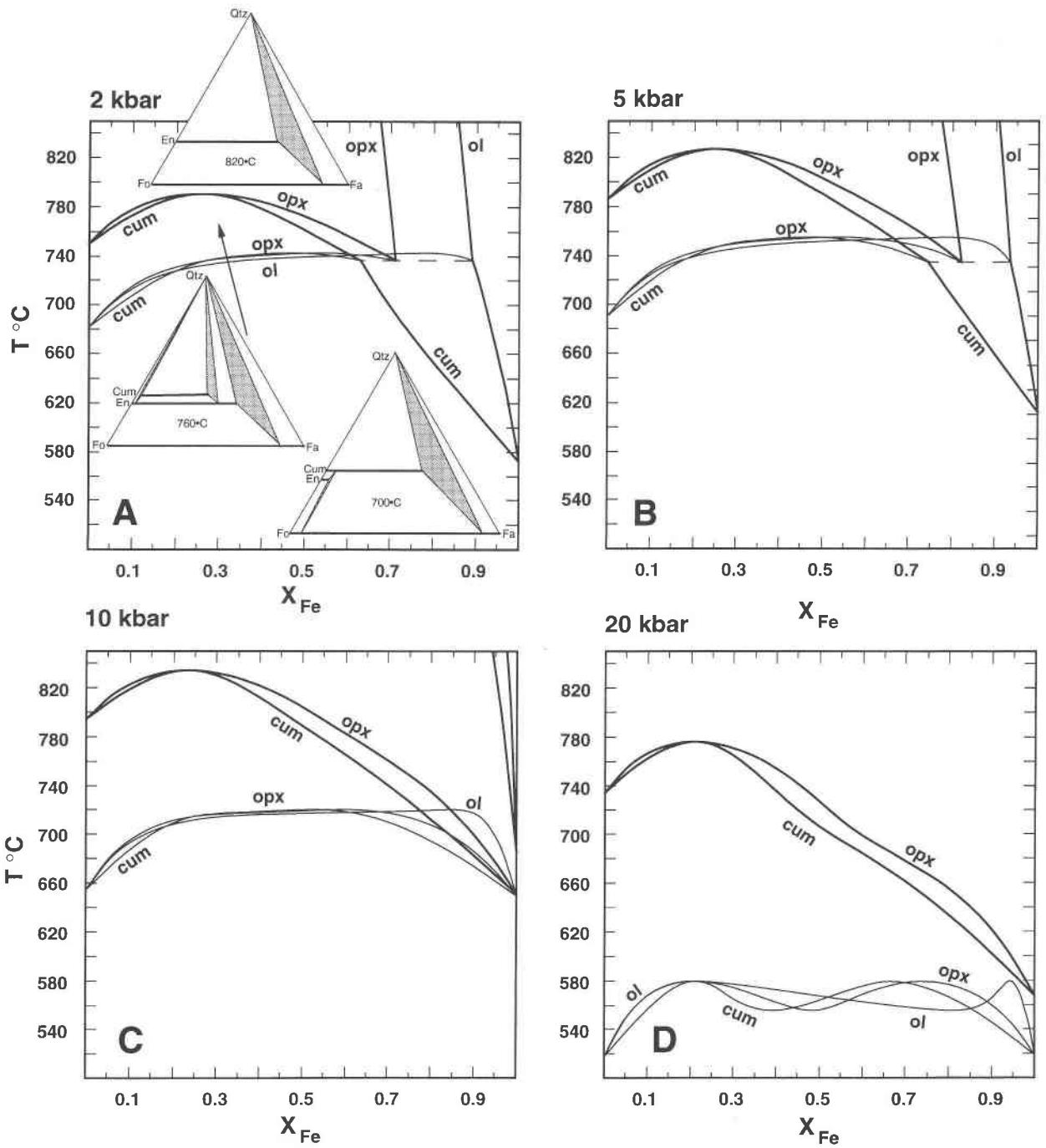

Fig. 5. T-X_{Fe} phase diagrams at 2 (**A**), 5 (**B**), 10 (**C**), and 20 kbar (**D**) and compatibilities at 2 kbar, showing the calculated stability limits of cummingtonite in the system FeO-MgO-SiO_2-H_2O, including the extremum in cummingtonite vs. orthopyroxene (+ quartz and H_2O). Note that anthophyllite takes the place of cummingtonite for $X_{Fe} < 0.10$ approximately at 700 °C and for more Fe-rich compositions at lower temperatures. At 20 kbar the diagram is in part metastable with respect to talc + orthopyroxene, and at low temperatures cummingtonite (or anthophyllite) is in part metastable with respect to talc + olivine.

Oxygen fugacity as a variable

All the above equilibria are oxygen-conserved and therefore independent of f_{O_2}. Nevertheless, those involving ferromagnesian olivine are constrained to f_{O_2} values somewhat below those of the NNO solid O_2 buffer by virtue of the equilibrium

$$\underset{\text{olivine}}{6Fe_2SiO_4} + O_2 = \underset{\text{orthopyroxene}}{6FeSiO_3} + \underset{\text{magnetite}}{2Fe_3O_4}. \quad (2)$$

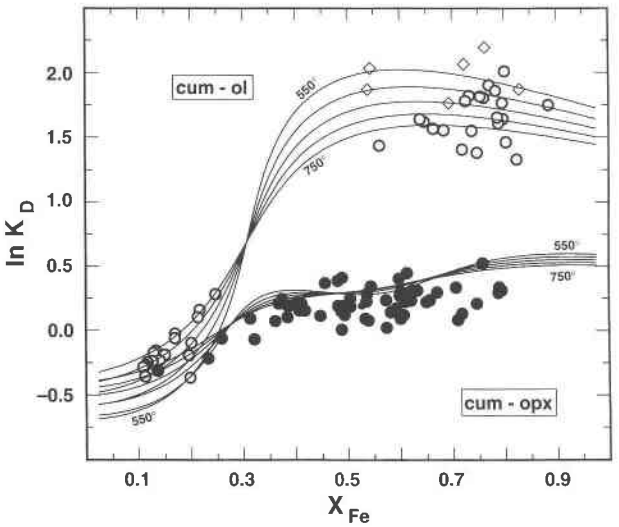

Fig. 6. Compilation from the literature of polythermal and polybaric Fe-Mg exchange equilibrium in natural cummingtonite + olivine (open circles) and cummingtonite + orthopyroxene pairs (solid circles), expressed as a function of X_{Fe} in cummingtonite. Open diamonds are Mn-rich cummingtonite + olivine compositions. Isotherms for 5 kbar calculated from Ghiorso et al. (1995). The value of $\ln K_D = (X_{Fe}/X_{Mg})^{Ol}/(X_{Fe}/X_{Mg})^{Cum}$ or $(X_{Fe}/X_{Mg})^{Opx}/(X_{Fe}/X_{Mg})^{Cum}$.

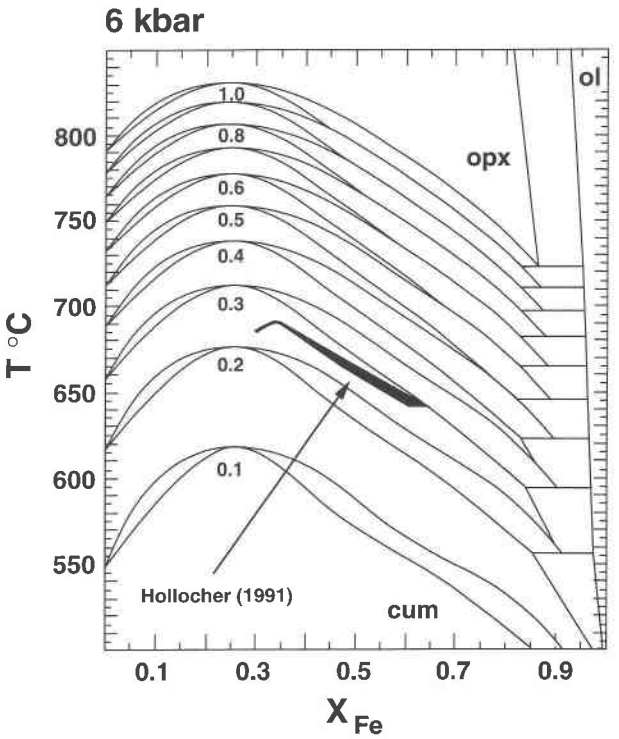

Fig. 7. Calculated T-X_{Fe} diagram for cummingtonite breakdown to orthopyroxene, quartz, and H_2O for activity of H_2O from 0.1 to 1.0. Estimated T-X_{Fe} field of cummingtonite + orthopyroxene in central Massachusetts amphibolites in black (Hollocher, 1991).

Ghiorso et al. (1995) illustrated the good agreement between calculated and experimentally determined X_{Fe} of cummingtonite at 4900 bars on the NNO buffer in the equilibrium

$$\underset{\text{cummingtonite}}{6Fe_7Si_8O_{22}(OH)_2} + 7O_2 = \underset{\text{magnetite}}{14Fe_3O_4} + \underset{\text{quartz}}{48SiO_2} + 6H_2O. \quad (3)$$

Figure 8 shows more detailed T-X_{Fe} relations at 2000 bars for the redox equilibria of cummingtonite, orthopyroxene, and olivine, contoured in units of log f_{O_2} > NNO and for the HM buffer. Reasonable agreement is found at the HM buffer with redox experiments on synthetic ferromagnesian amphibole by Popp et al. (1977). Anthophyllite and cummingtonite in this compositional and temperature range are energetically indistinguishable, so that ambiguity of experimental products in this context is unimportant and of less concern than the presence of chain-width errors and stacking faults, and the proper functioning of the HM solid O_2-buffer. The agreement is good on the NNO buffer (Fig. 8), particularly if we adopt our provisional data for anthophyllite.

Figure 9 depicts calculated relationships at four different pressures in terms of temperature and log f_{O_2} > NNO. In this plane, cummingtonite and orthopyroxene coexist with magnetite and quartz over wide ranges of f_{O_2} and temperature. Isopleths of cummingtonite composition (X_{Fe}) show that, at known T and P, the f_{O_2} of an aqueous pore fluid in a cummingtonite + magnetite + quartz rock may be determined quite precisely. Inasmuch as the compositions of cummingtonite in metamorphosed ironstones typically fall in the range X_{Fe} = 0.4–0.9, a relatively small range in log f_{O_2} values (<2 log units) is indicated. Cummingtonite in this assemblage becomes more magnesian with increasing temperature along the solid O_2 buffer curves, such as HM and NNO. Anthophyllite takes the place of magnesio-cummingtonite at high values of f_{O_2}, which correspond to low X_{Fe} in amphibole; Chakraborty (1963), Klein (1966), and Haase (1982a), for example, described anthophyllite [Fe/(Fe + Mg + Mn + Ca) = 0.17, 0.18, and 0.11, respectively] with hematite and quartz in high-Fe^{3+} metamorphosed iron formation. On the other hand, sample 10G of Mueller (1960) contains cummingtonite [Fe/(Fe + Mg + Mn + Ca) = 0.22] with magnetite, hematite, talc, and quartz. In the absence of magnetite or quartz, cummingtonite is stable to much lower values of log f_{O_2} than indicated by the isopleths in Figure 9.

In volcanic rocks, extensive use has been made of iron titanium oxide phenocrysts for thermometry and oxygen barometry, and some complete data sets are available for rhyolites and dacites containing both cummingtonite and orthopyroxene phenocrysts. An enlarged and modified version of Figure 9B at 2000 bars (Fig. 10) has been used to compare log f_{O_2} and T determined from the iron tita-

nium oxide phenocrysts (Ghiorso and Sack, 1991) and the X_{Fe} of cummingtonite, with predicted relationships for the assemblage cummingtonite + orthopyroxene + quartz + titanian magnetite (in equilibrium with ilmenite). The agreement is excellent, and we note especially the following: (1) the majority of samples defines a trend parallel to the calculated cummingtonite + orthopyroxene + magnetite + quartz curves; (2) measured X_{Fe} of cummingtonite [expressed as Fe/(Fe + Mg + Mn + Ca)] increases towards lower values of log f_{O_2} as predicted, and agrees with the calculated isopleths everywhere to within 0.02; and (3) at the total pressure of 2000 bars adopted for the diagram (consistent with 6–8 wt% Al_2O_3 in coexisting hornblende phenocrysts), the inferred activity of H_2O is 0.7–1.0, in good agreement with earlier estimates of high H_2O pressures accompanying cummingtonite-bearing volcanics (Ewart et al., 1971, 1975; Wood and Carmichael, 1973). Figure 10 also clearly shows how the accuracy of any estimate of H_2O activity is very much limited by that of the temperature estimate. Displacement of the model cummingtonite + orthopyroxene equilibrium in Figure 10, induced by impurities in natural pairs such as Al, Ca, and Mn, is quite small since these components are not strongly fractionated.

It is tempting from the quasi-linear trend of sample points in Figure 10 to view the coexistence of cummingtonite, orthopyroxene, quartz, and magnetite in siliceous volcanics as an O_2 buffer, driving f_{O_2} to lower values with declining temperature (and terminating with the crystallization of olivine, Fig. 9). The buffer reaction may be written with H_2 rather than O_2 to recognize the more abundant fluid species:

$$\underset{\text{orthopyroxene}}{5Fe_2Si_2O_6} + 2H_2O = \underset{\text{cummingtonite}}{Fe_7Si_8O_{22}(OH)_2} + \underset{\text{magnetite}}{Fe_3O_4} + \underset{\text{quartz}}{2SiO_2} + H_2. \quad (4)$$

However, unless accompanied by strong liquid-crystal fractionation, this assemblage probably has little buffer capacity in igneous systems because of the required increase in Fe/Mg ratios of the phases involved. The assemblage cummingtonite + olivine + quartz has not, to our knowledge, been found as phenocryst minerals in siliceous volcanics.

Cummingtonite phenocrysts in dacite at Saint Helens, Washington, have compositions [X_{Fe} expressed as Fe/(Fe + Mg + Mn + Ca)] of 0.42 (Klein, 1968) and 0.36, 0.31, 0.37, 0.34 (Smith and Leeman, 1982), which overlap those of cummingtonite in the Taupo Zone rhyolites. However, estimates of temperature (826 and 843 °C) and log f_{O_2} (ΔNNO = 1.7) based on the iron titanium oxides (Smith and Leeman, 1982; calibration of Ghiorso and Sack, 1991) are both high in comparison with those expected from the cummingtonite isopleths in Figure 10. Similarly, cummingtonite occurring as overgrowths on hornblende phenocrysts in the June 1991 dacite pumice of Pinatubo, Philippines (X_{Fe} = 0.29, Pallister et al., 1995; Rutherford and Devine, 1995), appears to be too Fe rich for the f_{O_2} derived from the iron titanium oxides (ΔNNO = 2.3–2.4). Given the agreement between calculated and measured X_{Fe} of cummingtonite, T, and log f_{O_2} for the Taupo Zone rhyolites, it seems very probable that the phenocryst phases in the Saint Helens and Pinatubo dacites are not all in frozen equilibrium. There is evidence for magma mixing in both the Pinatubo and Saint Helens dacites. Another possible explanation is a late increase in f_{O_2} in the magma that was recorded by the iron titanium oxides but not by the silicate phenocrysts.

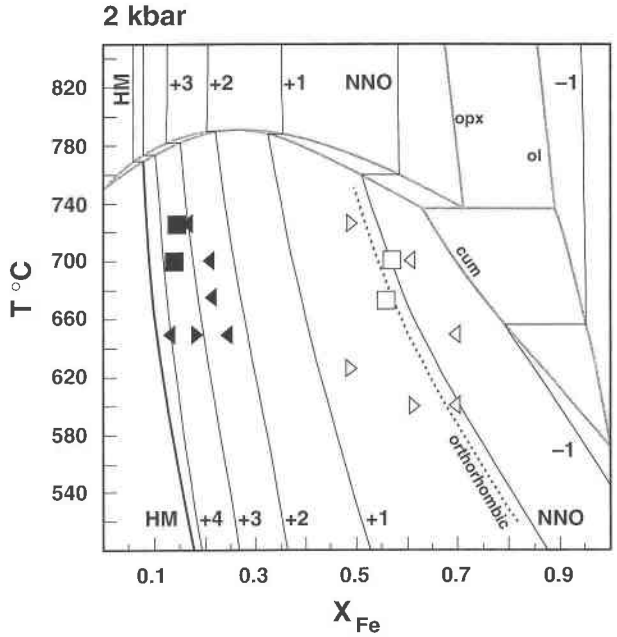

Fig. 8. Calculated T-X_{Fe} diagram at 2 kbar showing redox equilibria of cummingtonite, orthopyroxene, and olivine, with reference to log f_{O_2} defined by the NNO buffer. Arrows: reaction direction in experiments on "orthoamphibole" by Popp et al. (1977) on the HM buffer (solid symbols) and the NNO buffer (open symbols); squares: no change. Dotted: provisional calculated curve for orthoamphibole; on the HM buffer the curves for clino- and orthoamphibole are indistinguishable.

Experiments on natural dacites and rhyolites are mutually consistent in showing that cummingtonite has a maximum (760–800 °C) in its thermal stability at 2–3 kbar (Nicholls et al., 1992; Geschwind and Rutherford, 1992; Rutherford, 1993; Rutherford and Devine, 1995), apparently accompanied by a pronounced back bend in its limit between 3 and 4 kbar (Fig. 11). Our data on cummingtonite vs. orthopyroxene in FMSH reproduce the experimental cummingtonite-out curve reasonably well up to 3 kbar (the cummingtonite products were not analyzed), but the back bend could reflect continuation of the same equilibrium only if there were an accompanying major decrease in SiO_2 activity in the liquid with increase in pressure. The steep quartz-in curves for the rhyolites (Nicholls et al., 1992) suggest that this is not the case. Furthermore, the cummingtonite-in curve is not

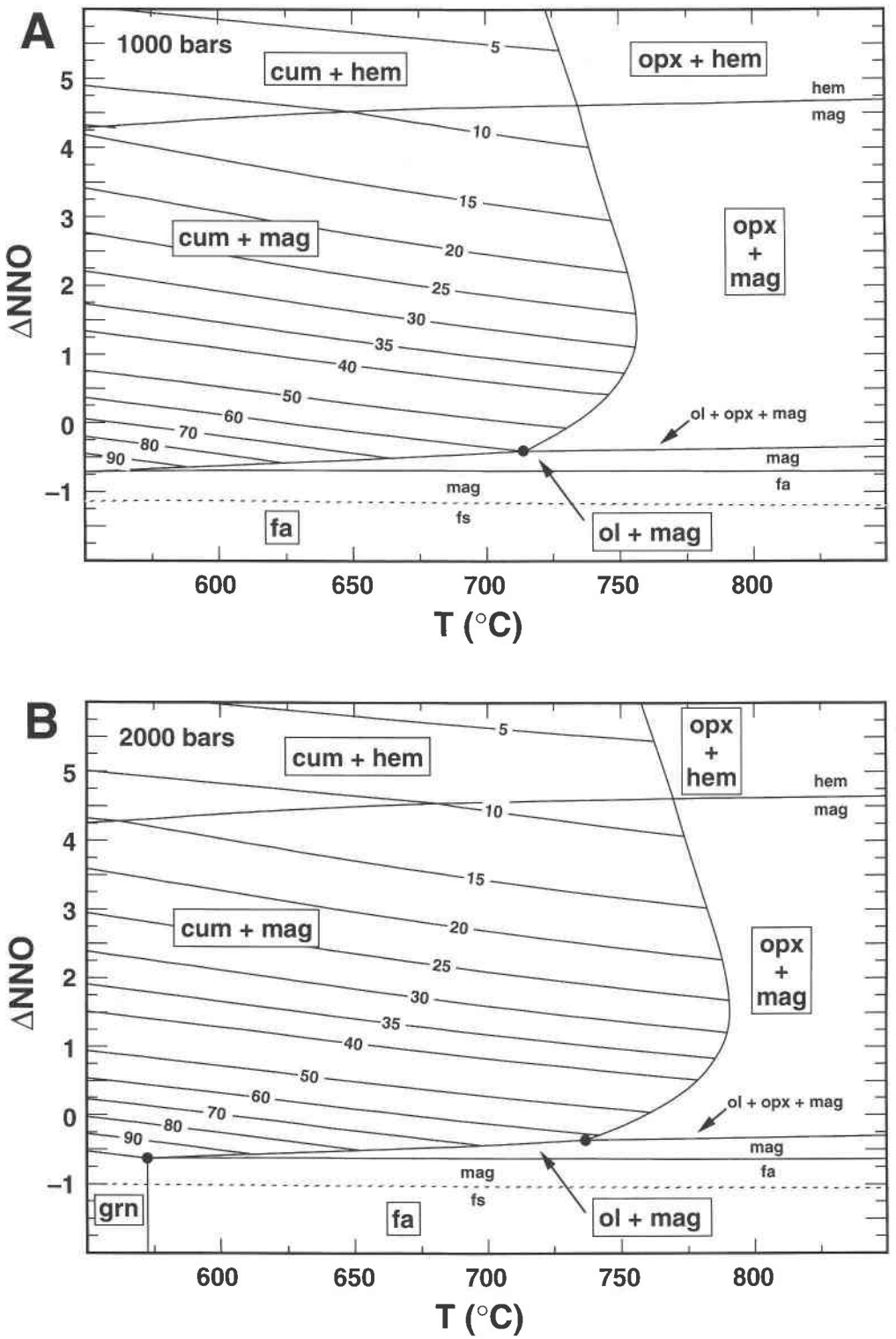

Fig. 9. Calculated T-$\Delta \log f_{O_2}$ ($\log f_{O_2}$ in excess of NNO) phase diagrams at 1 (**A**), 2 (**B**), 5 (**C**), and 10 kbar (**D**) illustrating redox and dehydration equilibria in the system FMSHO involving cummingtonite, olivine, orthopyroxene, magnetite, hematite, quartz, and H_2O. Depicts only quartz-saturated relations. Isopleths are percent grunerite in cummingtonite.

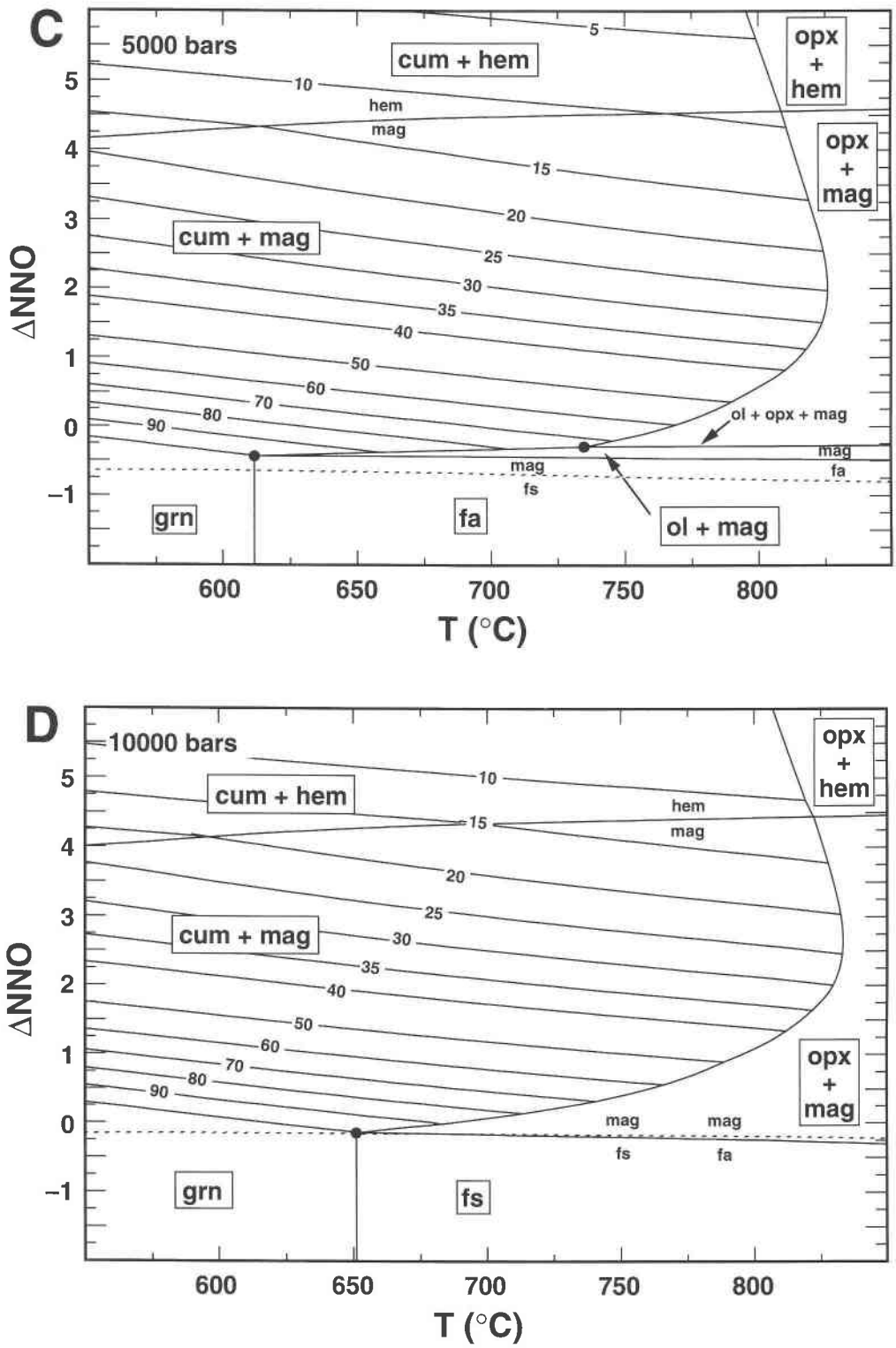

Fig. 9—*Continued.*

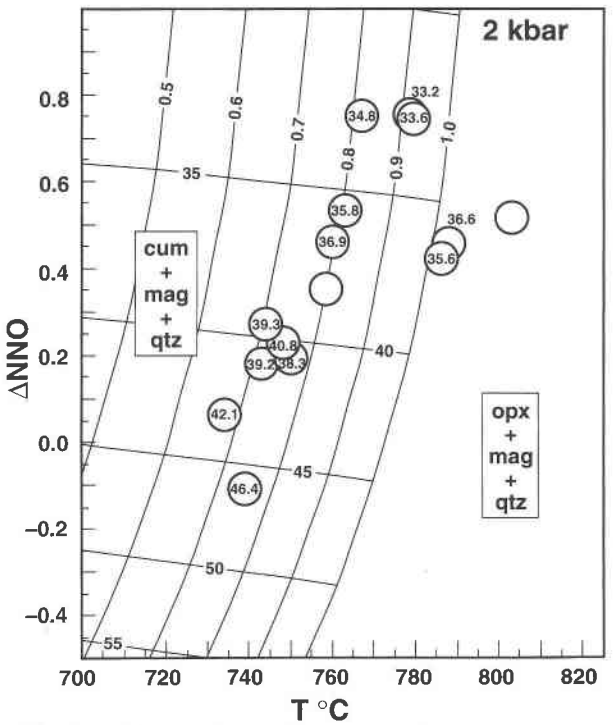

Fig. 10. Blowup of a modified version of Fig. 9B showing T, ΔNNO, and %Fe/(Fe + Mg + Mn + Ca) of natural cummingtonite (in circles) in cummingtonite-orthopyroxene rhyolites and dacites. Isopleths are calculated for a variable titaniferous magnetite composition in equilibrium with ilmenite. Contours 0.5–1.0 are activity of H_2O. Data on cummingtonite and iron titanium oxides from Ewart et al. (1971, 1975), Ewart (1994 personal communication), d'Arco et al. (1981), Pedersen and Hald (1982), and Ghiorso and Sack (1991, Table 1).

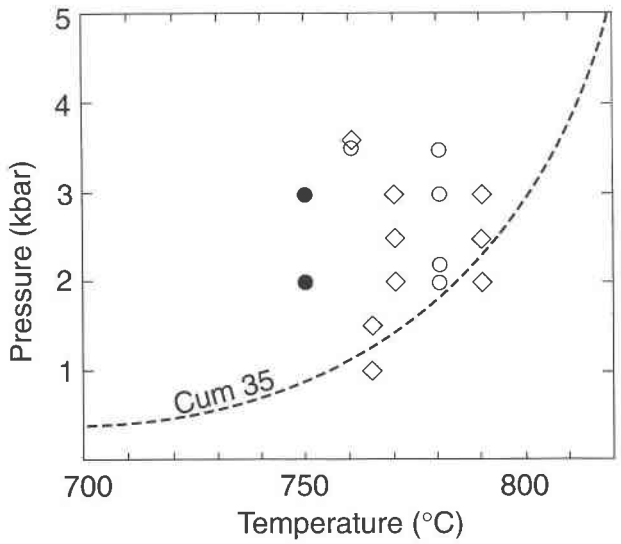

Fig. 11. Stability of cummingtonite in experiments on natural dacite (open circles and diamonds: Geschwind and Rutherford, 1992; Rutherford and Devine, 1995) and rhyolite (solid circles: Nicholls et al., 1992). Curve for stability limit of cummingtonite (35 percent grunerite) in the system FMSH from Fig. 4.

everywhere coincident in the experiments with an orthopyroxene-out curve. Therefore, there must be one or more other reactions in complex natural systems that restrict the stability of cummingtonite at pressures above 3–4 kbar in the 700–800 °C range. There seem to be at least two good possibilities, one involving reaction of cummingtonite with the components of plagioclase, and the other reaction of cummingtonite with the components of orthoclase.

The first is a reaction producing hornblende, which is written in terms of phase components in NCMFASH as

$$\underset{\text{cummingtonite}}{3(Mg,Fe)_7Si_8O_{22}(OH)_2} + \underset{\text{actinolite}}{7Ca_2(Mg,Fe)_5Si_8O_{22}(OH)_2} + \underset{\text{anorthite}}{14CaAl_2Si_2O_8} + \underset{\text{albite}}{14NaAlSi_3O_8} + 4H_2O = \underset{\text{pargasite}}{14NaCa_2(Mg,Fe)_4Al_3Si_6O_{22}(OH)_2} + 66SiO_2 \quad (5)$$

or in CMFASH as

$$\underset{\text{cummingtonite}}{3(Mg,Fe)_7Si_8O_{22}(OH)_2} + \underset{\text{anorthite}}{14CaAl_2Si_2O_8} + 4H_2O = \underset{\text{tschermakite}}{7Ca_2(Mg,Fe)_3Al_4Si_6O_{22}(OH)_2} + 10SiO_2. \quad (6)$$

Both reactions (which are not unlike the Al-in-hornblende barometer) have positive dP/dT slopes and proceed left to right with increase in pressure. They are relevant to amphibolites as well as to the volcanic rocks. Reaction 6 suggests that cummingtonite when present, for example, in Barrovian-style amphibolites should be accompanied by Na-rich plagioclase. Cummingtonite rims around hornblende and reverse-zoned plagioclase, suggesting progress to the left of Reaction 6, were described in amphibolite by Mottana et al. (1994).

The second possibility (perhaps more relevant to rhyolites) becomes clear when we examine the consequences of the intersection of the breakdown reaction of cummingtonite, with its steep dP/dT, and that of biotite + quartz, with its smaller dP/dT (Fig. 12). This intersection generates an even smaller dP/dT reaction:

$$\underset{\text{biotite}}{7K(Mg,Fe)_3AlSi_3O_{10}(OH)_2} + 24SiO_2 = 7KAlSi_3O_8 + \underset{\text{cummingtonite}}{3(Mg,Fe)_7Si_8O_{22}(OH)_2} + 4H_2O. \quad (7)$$

Figure 12 has been constructed with constant activities of phase components at values appropriate for dacites and rhyolites and is not intended to be read as a phase diagram showing stable relationships; depending on P and T, some of the phases would be undersaturated in silicic liquid. The disc-shaped field for orthoclase + cummingtonite + H_2O must apply, albeit with some modification for P-T–dependent variation in activities, as a constraint

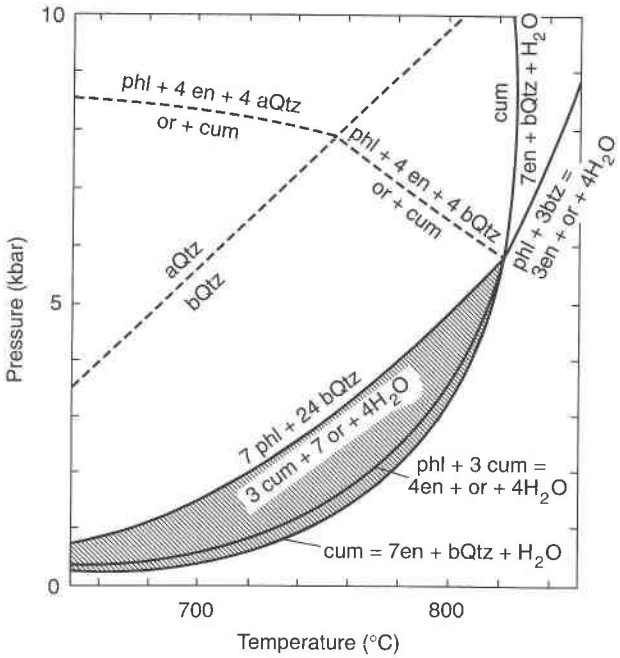

Fig. 12. Topology of equilibria among the phase components enstatite (a = 0.62), magnesio-cummingtonite (a = 0.028), phlogopite (a = 0.216), and orthoclase (a = 0.4), together with quartz and H_2O. Curves are metastable with respect to silicic liquid over much of the diagram. Ruled field represents cummingtonite + orthoclase for the adopted activities.

on the crystallization of cummingtonite in siliceous magmas.

Cummingtonite-bearing volcanic rocks are indicative of shallow magma chambers (<4 kbar) and H_2O-rich fluid close to or at saturation, and typically large volumes of magma are involved. It comes as no surprise then that the eruption of such magmas releases enormous amounts of energy (e.g., Walker, 1980).

Although Reaction 7 as written is a subsolidus dehydration reaction, it is a close approximation of the melting reaction inferred by Kenah and Hollister (1983) to have proceeded left to right in migmatitic gneiss in northern British Columbia. It raises the possibility that the reaction may just as well have been a consequence of decompression as much as the final temperature increment in the metamorphism as they suggested. For assemblages saturated in orthoclase the field of cummingtonite + orthoclase is smaller than indicated in Figure 12. This no doubt explains why the paragenesis cummingtonite + potassium feldspar has apparently not been found in metamorphic rocks (P. Robinson, 1994 personal communication).

Metamorphic thermobarometry

The near-binary character of metamorphic cummingtonite offers advantages over most calcic amphiboles for purposes of thermobarometry in that measured compositions translate with minor correction into activities of

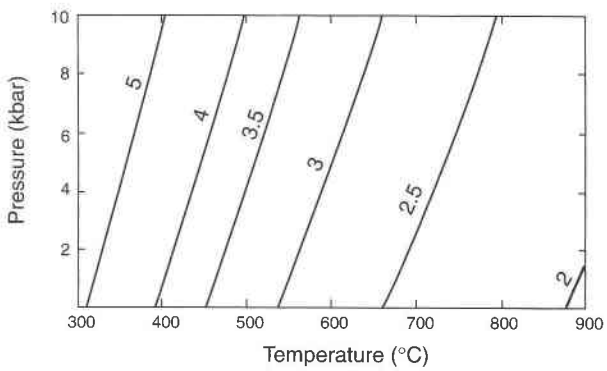

Fig. 13. Temperature and pressure dependence of K for the exchange equilibrium ⅓pyrope + ½grunerite = ⅓almandine + ½magnesio-cummingtonite.

phase components. Cureton and Essene (1994) have proposed the Fe end-member equilibrium

$$\text{grunerite} + \text{anorthite} = \text{grossular} + \text{almandine} + \text{quartz} + H_2O \quad (8)$$

as a barometer. This equilibrium is preserved in many rock types in amphibolite facies terrains. If we expand it into the system CFMASH, it has potential, among other things, as a test of thermodynamic models for the Fe and Mg components of garnet and cummingtonite.

The temperature dependence of Fe-Mg exchange between cummingtonite and olivine or orthopyroxene is too small to offer any serious possibility for thermometry (Fig. 6). However, Fe-Mg exchange with garnet has much greater potential (Fig. 13), and again the problem of complex substitutions in calcic amphibole is avoided (cf. the hornblende-garnet thermometer, Graham and Powell, 1984).

Extension to more complex amphiboles

The formulation of a satisfactory solution model for the cummingtonite series represents an initial step in the development of a thermodynamic model for more complex amphiboles that derive from the cummingtonite base by means of some simple exchanges or reconstructive transformations. At least the quadrilateral clinoamphiboles and the anthophyllite-gedrite series are likely to be readily accessed in this way.

Acknowledgments

We acknowledge the efforts of Marc Hirschmann and Hexiong Yang, who performed the single-crystal X-ray work on which this study is based. We thank E.J. Essene, B.R. Frost, R. Popp, and M.J. Rutherford for comments and reviews. Support from the National Science Foundation through grants EAR-9104714 and EAR-9303972 is greatly appreciated. Computations were facilitated by a generous grant from Digital Equipment Corporation.

References cited

Berg, J.H. (1977) Dry granulite mineral assemblages in the contact aureoles of the Nain Complex, Labrador. Contributions to Mineralogy and Petrology, 64, 33–52.

Berman, R.G. (1988) Internally-consistent thermodynamic data for minerals in the system Na_2O-K_2O-CaO-MgO-FeO-Fe_2O_3-Al_2O_3-SiO_2-TiO_2-H_2O-CO_2. Journal of Petrology, 29, 445–522.

Besancon, J.R. (1991) Orthopyroxene Fe/Mg order-disorder estimated from chemical composition and optic axial angle ($2V_x$). Geological Society of America Abstracts with Programs, 23, A220.

Bohlen, S.R., and Essene, E.J. (1978) The significance of metamorphic fluorite in the Adirondacks. Geochimica et Cosmochimica Acta, 42, 1669–1678.

Bohlen, S.R., Essene, E.J., and Boettcher, A.L. (1980) Reinvestigation and application of olivine-quartz-orthopyroxene barometry. Earth and Planetary Science Letters, 47, 1–10.

Bonnichsen, B. (1969) Metamorphic pyroxenes and amphiboles in the Biwabik Iron Formation, Dunka River Area, Minnesota. Mineralogical Society of America Special Paper, 2, 217–239.

Bowen, N.L., and Schairer, J.F. (1935) Grünerite from Rockport, Massachusetts, and a series of synthetic fluor-amphiboles. American Mineralogist, 20, 543–551.

Bown, M.G. (1966) A new amphibole polymorph in intergrowth with tremolite: Clino-anthophyllite? American Mineralogist, 51, 259–260.

Carpenter, M.A. (1982) Amphibole microstructures: Some analogies with phase transformations in pyroxenes. Mineralogical Magazine, 36, 395–397.

Chakraborty, K.L. (1963) Ferromagnesian silicate minerals in the metamorphosed iron-formations of Wabash Lake and adjacent areas, Newfoundland and Quebec. Geological Society of Canada Bulletin, 143, 34 p.

Cureton, J.S., and Essene, E.J. (1994) Cummingtonite-plagioclase-garnet-quartz: A new geobarometer for amphibolites. Geological Society of America Abstracts with Programs, 26(7), A-43.

d'Arco, P., Maury, R.C., and Westercamp, D. (1981) Geothermometry and geobarometry of a cummingtonite-bearing dacite from Martinique, Lesser Antilles. Contributions to Mineralogy and Petrology, 77, 177–184.

De Capitani, L., and Liborio, G. (1990) Cummingtonite nelle plutoniti della Val Biandino (Como). Rendiconti Lincei Scienze Fisiche e Naturale, series 9, vol. 1, 379–385.

Droop, G.T.R. (1994) Triple-chain pyriboles in Lewisian ultramafic rocks. Mineralogical Magazine, 58, 1–20.

Dymek, R.F., Brothers, S.C., and Schiffries, C.M. (1988) Petrogenesis of ultramafic metamorphic rocks from the 3800 Ma Isua Supracrustal Belt, West Greenland. Journal of Petrology, 29, 1353–1397.

Evans, B.W. (1982) Amphiboles in metamorphosed ultramafic rocks. In Mineralogical Society of America Reviews in Mineralogy, 9B, 98–112.

——— (1986) Reactions among sodic, calcic, and ferromagnesian amphiboles, sodic pyroxene, and deerite in high-pressure metamorphosed ironstone, Siphnos, Greece. American Mineralogist, 71, 1118–1125.

Ewart, A., Green, D.C., Carmichael, I.S.E., and Brown, F.H. (1971) Voluminous low temperature rhyolitic magmas in New Zealand. Contributions to Mineralogy and Petrology, 33, 128–144.

Ewart, A., Hildreth, W., and Carmichael, I.S.E. (1975) Quaternary acid magma in New Zealand. Contributions to Mineralogy and Petrology, 51, 1–27.

Ferry, J.M. (1994) A historical review of metamorphic fluid flow. Journal of Geophysical Research, 99(B8), 15487–15498.

Floran, R.J., and Papike, J.J. (1978) Mineralogy and petrology of the Gunflint Iron-formation, Minnesota-Ontario: Correlation of compositional and assemblage variations at low to moderate grade. Journal of Petrology, 19, 215–288.

Fonarev, V.I. (1987) Mineral equilibria of Precambrian iron formations, p. 294. Nauka, Moscow (in Russian).

Geschwind, C., and Rutherford, M.J. (1992) Cummingtonite and the evolution of the Mt. Helens (Washington) magma system: An experimental study. Geology, 20, 1011–1014.

Ghiorso, M.S., and Sack, R.O. (1991) Fe-Ti oxide geothermometry: Thermodynamic formulation and the estimation of intensive variables in silicic magmas. Contributions to Mineralogy and Petrology, 108, 485–510.

Ghiorso, M.S., Evans, B.W., Hirschmann, M.M., and Yang, H. (1995) Thermodynamics of the amphiboles: Fe-Mg cummingtonite solid solutions. American Mineralogist, 80, 502–519.

Ghose, S., and Weidner, J. (1972) Mg^{2+}-Fe^{2+} order-disorder in cummingtonite, $(Mg,Fe)_7Si_8O_{22}(OH)_2$: A new geothermometer. Earth and Planetary Science Letters, 16, 346–354.

Gole, M.J., and Klein, C. (1981) High-grade metamorphic Archean banded iron formations, West Australia: Assemblages with coexisting pyroxenes ± fayalite. American Mineralogist, 66, 87–99.

Graham, C.M., and Powell, R. (1984) A garnet-hornblende geothermometer: Calibration, testing, and application to the Pelona Schist, Southern California. Journal of Metamorphic Geology, 2, 13–21.

Grant, C.A., and Dyar, M.D. (1994) Sources of experimental and analytical error in measurements of the Mössbauer effect in amphibole. Geological Society of America Abstracts with Programs, 26(7), A-166.

Haase, C.S. (1982a) Metamorphic petrology of the Negaunee Iron Formation, Marquette District, Northern Michigan: Mineralogy, metamorphic reactions and phase equilibria. Economic Geology, 77, 60–81.

——— (1982b) Phase equilibria in metamorphosed iron-formations: Qualitative T-$X(CO_2)$ petrogenetic grids. American Journal of Science, 282, 1623–1654.

Hafner, S.S., and Ghose, S. (1971) Iron and magnesium distribution in cummingtonites $(Fe,Mg)_7Si_8O_{22}(OH)_2$. Zeitschrift für Kristallographie, 133, 301–326.

Hawthorne, F.C. (1983) Quantitative characterization of site-occupancies in minerals. American Mineralogist, 68, 287–306.

Hirschmann, M., Evans, B.W., and Yang, H. (1994) Composition and temperature dependence of Fe-Mg ordering in cummingtonite-grunerite as determined by X-ray diffraction. American Mineralogist, 79, 862–877.

Hollocher, K. (1991) Prograde amphibole dehydration reactions during high-grade regional metamorphism, central Massachusetts, U.S.A. American Mineralogist, 76, 956–970.

Hoschek, G. (1976) Melting relations of biotite + plagioclase + quartz. Neues Jahrbuch für Mineralogie Monatshefte, 2, 79–83.

Kenah, C., and Hollister, L. (1983) Anatexis in the Central Gneiss Complex, British Columbia. In M. Atherton and C. Gribble, Eds., Migmatites, melting and metamorphism, p. 142–161. Nantwich, Cheshire, U.K.

Kisch, H.J. (1969) Magnesio-cummingtonite, $P2_1/m$: A Ca- and Mn-poor clinoamphibole from New South Wales. Contributions to Mineralogy and Petrology, 21, 319–331.

Klein, C., Jr. (1966) Mineralogy and petrology of the metamorphosed Wabash Iron Formation, Southwestern Labrador. Journal of Petrology, 7, 246–305.

——— (1968) Coexisting amphiboles. Journal of Petrology, 9, 281–330.

——— (1982) Amphiboles in iron-formation. In Mineralogical Society of America Reviews in Mineralogy, 9B, 88–98.

Leake, B.E. (1978) Nomenclature of amphiboles. Mineralogical Magazine, 42, 533–563.

Lattard, D., and Evans, B.W. (1992) New experiments on the stability of grunerite. European Journal of Mineralogy, 4, 219–238.

Lattard, D., and Le Breton, N. (1993) the P-T-f_{O_2} stability of deerite, $Fe^{2+}_{12}Fe^{3+}_8[Si_{12}O_{40}](OH)_{10}$. Contributions to Mineralogy and Petrology, 115, 474–487.

Matthes, S. (1986) Die prograde Kontaktmetamorphose von Serpentin des Oberpfälzer Waldes. Geologica Bavarica, 89, 7–20.

Mottana, A., Bocchio, R., Crespi, R., De Capitani, L., Liborio, G., and Della Ventura, G. (1994) Cummingtonite in the amphibolites of the South-Alpine Basement Complex (Upper Lake Como Region, Italy): Its relationships with hornblende. Mineralogy and Petrology, 51, 67–84.

Miyano, T., and Klein, C., Jr. (1986) Fluid behavior and phase relations in the system Fe-Mg-Si-C-O-H: Application to high grade metamorphism of iron formations. American Journal of Science, 286, 540–575.

Morey, G.B., Papike, J.J., and Smith, R.W. (1972) Observations on the contact metamorphism of the Biwabik Iron Formation, East Mesabi District, Minnesota. Geological Society of America Memoir, 135, 225–263.

Mueller, R.F. (1960) Compositional characteristics and equilibrium relations in mineral assemblages of a metamorphosed iron formation. American Journal of Science, 258, 449–497.

Nicholls, I.A., Oba, T., and Conrad, W.K. (1992) The nature of primary rhyolitic magmas involved in crustal evolution: Evidence from an experimental study of cummingtonite-bearing rhyolites, Taupo Volcanic Zone, New Zealand. Geochimica et Cosmochimica Acta, 56, 955–962.

Pallister, J.S., Hoblitt, R.P., Meeker, G.P., Newhall, C.G., Knoght, R.J.,

and Siems, D.F. (1995) Magma mixing at Pinatubo Volcano: Petrographic and chemical evidence from the 1991 deposits. In U.S. Geological Survey Special Publication, in press.

Pedersen, A.K., and Hald, N. (1982) A cummingtonite porphyritic dacite with amphibole-rich xenoliths from the Tertiary central volcano at Kroksfjordur, N.W. Iceland. Lithos, 15, 137–159.

Pfeifer, H.R. (1979) Fluid-Gesteins-Interaktion in metamorphen Ultramafititen der Zentralalpen, 200 p. Doctoral dissertation no. 6379, Eidgenossiche Technische Hochschule, Zurich.

Popp, R.K., Gilbert, M.C., and Craig, J.R. (1977) Stability of Fe-Mg amphiboles with respect to oxygen fugacity. American Mineralogist, 62, 1–12.

Press, W.H., Flannery, B.P., Teukolsky, S.A., and Vetterling, W.T. (1990) Numerical recipes in C, 735 p. Cambridge University Press, Cambridge, U.K.

Prewitt, C.T., Ross, M., and Clark, J.R. (1970) Cummingtonite: A reversible, nonquenchable transition from $P2_1/m$ to $C2/m$ symmetry. Earth and Planetary Science Letters, 8, 448–450.

Rice, J.M., Evans, B.W., and Trommsdorff, V. (1974) Widespread occurrence of magnesiocummingtonite, Cima di Gagnone, Ticino, Switzerland. Contributions to Mineralogy and Petrology, 43, 245–251.

Ross, M., Papike, J.J, and Shaw, K.W. (1969) Exsolution textures in amphiboles as indicators of subsolidus thermal histories. Mineralogical Society of America Special Paper, 2, 275–299.

Rutherford, M.J. (1993) Experimental petrology applied to volcanic processes. Eos, 74, 49 and 55.

Rutherford, M.J., and Devine, J.D. (1995) Pre-eruption pressure-temperature conditions and volatiles in the 1991 dacitic magma of Mount Pinatubo. In U.S. Geological Survey Special Publication, in press.

Sack, R.O., and Ghiorso, M.S. (1989) Importance of considerations of mixing properties in establishing an internally consistent thermodynamic database: Thermochemistry of minerals in the system Mg_2SiO_4-Fe_2SiO_4-SiO_2. Contributions to Mineralogy and Petrology, 102, 41–68.

——— (1994) Thermodynamics of multicomponent pyroxenes: II. Phase relations in the quadrilateral. Contributions to Mineralogy and Petrology, 116, 287–300.

Savko, K.A. (1994) Fayalite-grunerite-magnetite-quartz rocks of the Voronezh Crystalline Massif Iron Formation: Phase equilibria and metamorphic conditions. Petrology, 2, 482–493 (translated from Petrologiya, 2, 540–550).

Schneidermann, J.S., and Tracy, R.J. (1991) Petrology of orthoamphibole-cordierite gneisses from the Orijärvi area, southwest Finland. American Mineralogist, 76, 942–955.

Seifert, F. (1978) Equilibrium Mg-Fe^{2+} cation distribution in anthophyllite. American Journal of Science, 278, 1323–1333.

Seifert, F., and Virgo, D. (1975) Temperature dependence of intracrystalline Fe^{2+}-Mg distribution in a natural anthophyllite. Carnegie Institution of Washington Year Book, 73, 405–411.

Sharp, Z.D., and Essene, E.J. (1991) Metamorphic conditions of an Archean Core Complex in the northern Wind River Range, Wyoming. Journal of Petrology, 32, 241–273.

Simmons, E.C., Lindsley, D.H., and Papike, J.J. (1974) Phase relations and crystallization sequence in a contact metamorphosed rock from the Gunflint Iron Formation, Minnesota. Journal of Petrology, 15, 539–565.

Smith, D.R., and Leeman, W.P. (1982) Mineralogy and phase chemistry of Mt. St. Helens tephra sets W and Y as keys to their identification. Quaternary Research, 17, 211–227.

Tarasov, V.I., and Nikitina, L.P. (1974) Concerning the potential use of optic axial angle and unit cell parameters as criteria of ordering of Fe^{2+} and Mg in the structure of orthorhombic pyroxene. Zapiski Vsesoyuznogo Mineralogichskogo Obshchestva, 103, 268–271 (in Russian).

Tarasov, V.I., Nikitina, L.P., and Ekimov, S.N. (1975) Crystal-optic and X-ray methods of determination of cation ordering in the structure of orthorhombic pyroxenes. Zapiski Vsesoyuznogo Mineralogichskogo Obshchestva, 104, 748–750 (in Russian).

Vaniman, D.T., Papike, J.J., and Labotka, T. (1980) Contact-metamorphic effects of the Stillwater Complex, Montana: The concordant iron formation. American Mineralogist, 65, 1087–1102.

Walker, G.P.L. (1980) The Taupo plinian pumice: Product of the most powerful known (ultraplinian) eruption? Journal of Volcanology and Geothermal Research, 8, 69–94.

Wood, B.J., and Carmichael, I.S.E. (1973) P_{total}, P_{H_2O} and the occurrence of cummingtonite in volcanic rocks. Contributions to Mineralogy and Petrology, 40, 149–158.

Yang, H., and Hirschmann, M. (1995) Crystal structure of $P2_1/m$ ferromagnesian amphibole and the role of cation ordering and composition in the $P2_1/m$-$C2/m$ transition in cummingtonite. American Mineralogist, 80, in press.

Manuscript received March 8, 1995
Manuscript accepted April 13, 1995